

Thermoelectric properties of finite two-dimensional quantum dot arrays with band-like electronic states

David M T Kuo

Department of Electrical Engineering and Department of Physics,
National Central University, Chungli, 320 Taiwan

(Dated: May 26, 2020)

The thermal power ($PF = S^2 G_e$) depends on the Seebeck coefficient (S) and electron conductance (G_e). The enhancement of G_e will unavoidably suppress S because they are closely related. As a consequence, the optimization of PF is extremely difficult. Here, we theoretically investigated the thermoelectric properties of two-dimensional quantum dot (QD) arrays with carriers injected from electrodes. The Lorenz number of 2D QD arrays in the resonant tunneling procedure satisfies the Wiedemann-Franz law, which confirms the formation of minibands. When the miniband center is far away from the Fermi level of the electrodes, the electron transport is in the thermionic-assisted tunneling procedure (TATP). In this regime, G_e in band-like situation and S in atom-like situation can happen simultaneously. We have demonstrated that the enhancement of G_e with an increasing number of electronic states will not suppress S in the TATP.

I. INTRODUCTION

The semiconductor quantum dots (QDs) resulting from the quantum confinement of heterostructures exhibit atom-like discrete electron energy levels. High-efficiency single-QD devices show the functionalities of low electrical and optical power outputs. These single-QD devices include single electron transistors[1-3], single photon sources[4-6], single photon detectors[7] and single electron heat engines[8]. Some applications of QD devices require both high efficiency and significant output power. Therefore, one needs QD solids that can retain the size tunable properties of the QDs while exhibiting the band transport characteristic of bulk semiconductors.[9] Although much effort has been devoted to producing such QD solids, studies of the thermoelectric properties of such 2D QD arrays have been lacking.[10,11]

Designing a thermoelectric material with a high figure of merit (ZT) and optimized power output is under pursuit.[12-14] The dimensionless figure of merit $ZT = S^2 G_e T / \kappa$ depend on the Seebeck coefficient (S), electrical conductance (G_e) and thermal conductance (κ) of the material. Although 1D QD arrays have very high ZT values, there exist many limitations in the implementations of thermoelectric devices.[9] 2D and 3D QD arrays are required for realistic applications. The κ of a 2D QD array is smaller than that of bulk material.[15] This low dimensional system has the potential to realize high ZT values.[16] Therefore, it is desirable to investigate the power factor ($PF = S^2 G_e$) of 2D QD arrays, which directly affects the electrical power output. The enhancement of G_e calls for a large number of electronic states (band-like). However a large S value occurs in dilute electronic states (atom-like). Therefore, enhancing one of these physical quantities will unavoidably suppress the other. This study theoretically investigated the thermoelectric properties of a finite 2D QD array coupled to electrodes, as shown in Fig. 1. The electrons of the QD array are injected from the electrodes.[17] We demonstrated that G_e in band-like situation and S in atom-

like situation can happen simultaneously when the miniband center of a 2D QD array remains a certain distance from the Fermi level of the electrodes. These results will improve the thermoelectric performance of 2D materials such as $SnSe$ and MoS_2 . [18-20]

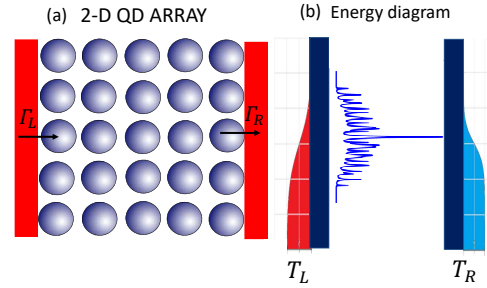


FIG. 1: (a) Schematic diagram of a two dimensional (2D) quantum dot (QD) array coupled to electrodes. Γ_L (Γ_R) denotes the tunneling rate of the electrons between the left (right) electrode and the leftmost (rightmost) QDs. Energy diagram of a 2D QD array coupled to electrodes with different equilibrium temperatures (T_L and T_R).

II. FORMALISM

To model the thermoelectric properties of a 2D QD array connected to the electrodes, the Hamiltonian of the system shown in Fig. 1 is given by $H = H_0 + H_{QD}$, [21] where

$$H_0 = \sum_{k,\sigma} \epsilon_k a_{k,\sigma}^\dagger a_{k,\sigma} + \sum_{k,\sigma} \epsilon_k b_{k,\sigma}^\dagger b_{k,\sigma} \quad (1)$$

$$+ \sum_{\ell} \sum_{k,\sigma} V_{k,\ell,j}^L d_{\ell,j,\sigma}^\dagger a_{k,\sigma} + \sum_{\ell} \sum_{k,\sigma} V_{k,\ell,j}^R d_{\ell,j,\sigma}^\dagger b_{k,\sigma} + H.c.$$

The first two terms of Eq. (1) describe the free electron gas in the left and right electrodes. $a_{k,\sigma}^\dagger$ ($b_{k,\sigma}^\dagger$) creates

an electron of momentum k and spin σ with energy ϵ_k in the left (right) electrode. $V_{k,\ell,j}^L$ ($V_{k,\ell,j}^R$) describes the coupling between the left (right) lead with its adjacent QD in the ℓ th row, which counts from 1 to N_y .

$$H_{QD} = \sum_{\ell,j,\sigma} E_{\ell,j} d_{\ell,j,\sigma}^\dagger d_{\ell,j,\sigma} \quad (2)$$

$$+ \sum_{\sigma} \sum_{\ell_1,\ell_2} \sum_{j_1,j_2}^{N_y, N_x} t_{\ell_1,\ell_2,j_1,j_2} d_{\ell_1,j_1,\sigma}^\dagger d_{\ell_2,j_2,\sigma} + H.c.,$$

$$t_{\ell_1,\ell_2,j_1,j_2} = \begin{cases} -t_y & \text{if } j_1 = j_2, |\ell_1 - \ell_2| = 1 \\ -t_x & \text{if } \ell_1 = \ell_2, |j_1 - j_2| = 1 \end{cases}, \quad (3)$$

where $E_{\ell,j}$ is the energy level of QD in the ℓ -th row and j -th column. The spin-independent $t_{\ell_1,\ell_2,j_1,j_2}$ describes the electron hopping strength, which is limited to the nearest neighboring sites. $d_{\ell_1,j_1,\sigma}^\dagger$ ($d_{\ell_2,j_2,\sigma}$) creates (destroys) one electron in the QD at the ℓ th row and j th column. If the wave functions of the electrons in each QD are localized, the electron Coulomb interactions are strong. Their effects on electron transport are significant in the scenario of weak hopping strengths.[22] On the other hand, the wave functions of the electrons are delocalized in the scenario of strong hopping strengths to form minibands; hence their weak electron Coulomb interactions can be ignored.

To study the transport properties of a 2D QD array junction connected to electrodes, it is convenient to use the Keldysh-Green's function technique[21,23]. Electron and heat currents leaving electrodes can be expressed as

$$J = \frac{2e}{h} \int d\varepsilon T_{LR}(\varepsilon) [f_L(\varepsilon) - f_R(\varepsilon)], \quad (4)$$

and

$$Q_{e,L(R)} = \frac{\pm 2}{h} \int d\varepsilon T_{LR}(\varepsilon) (\varepsilon - \mu_{L(R)}) [f_L(\varepsilon) - f_R(\varepsilon)] \quad (5)$$

where $f_\alpha(\varepsilon) = 1/\{\exp[(\varepsilon - \mu_\alpha)/k_B T_\alpha] + 1\}$ denotes the Fermi distribution function for the α -th electrode, where μ_α and T_α are the chemical potential and the temperature of the α electrode. e , h , and k_B denote the electron charge, the Planck's constant, and the Boltzmann constant, in that order. $T_{LR}(\varepsilon)$ denotes the transmission coefficient of a 2D QD array connected to electrodes, which can be solved by the formula $T_{LR}(\varepsilon) = 4Tr[\hat{\Gamma}_L \hat{G}_{D,A}^r(\varepsilon) \hat{\Gamma}_R \hat{G}_{D,A}^a(\varepsilon)]$, where the matrix of tunneling rates ($\hat{\Gamma}_L$ and $\hat{\Gamma}_R$) and Green's functions ($\hat{G}_{D,A}^r(\varepsilon)$ and $\hat{G}_{D,A}^a(\varepsilon)$) can be constructed by coding.[24]

The electrical conductance (G_e), Seebeck coefficient (S) and electron thermal conductance (κ_e) can be evaluated by using Eqs. (4) and (5) with a small applied bias $\Delta V = (\mu_L - \mu_R)/e$ and cross-junction temperature difference $\Delta T = T_L - T_R$. We obtain these thermoelectric coefficients $G_e = e^2 \mathcal{L}_0$, $S = -\mathcal{L}_1/(eT\mathcal{L}_0)$ and

$\kappa_e = \frac{1}{T}(\mathcal{L}_2 - \mathcal{L}_1^2/\mathcal{L}_0)$. \mathcal{L}_n is given by

$$\mathcal{L}_n = \frac{2}{h} \int d\varepsilon T_{LR}(\varepsilon) (\varepsilon - E_F)^n \frac{\partial f(\varepsilon)}{\partial E_F}, \quad (6)$$

where $f(\varepsilon) = 1/(\exp^{(\varepsilon - E_F)/k_B T} + 1)$ is the Fermi distribution function of electrodes at equilibrium temperature T .

III. RESULTS AND DISCUSSION

According to Eq. (6), transmission coefficient plays a significant role for electron transport between the electrodes. To illustrate the electronic states of finite 2D QD array, we have calculated and shown in Fig. 2 transmission coefficient $T_{LR}(\varepsilon)$ as a function of ε for different tunneling rates ($\Gamma_{L(R),\ell,j}(\varepsilon) = 2\pi \sum_k |V_{k,\ell,j}^{L(R)}|^2 \delta(\varepsilon - \varepsilon_k) = \Gamma_t$). A square lattice with homogenous electron hopping strengths $t_x = t_y = t_c = 6\Gamma_0$ and site-independent QD energy level $E_{\ell,j} = E_0 = E_F$ has been considered in the calculation of $T_{LR}(\varepsilon)$. All physical parameters are in units of Γ_0 . In Fig. 2(a), $T_{LR}(\varepsilon)$ reveals the tunneling probability of the electrons of the electrodes through the electronic states of 2D QD array, those energy is described by $\varepsilon = E_0 - 2t_c(\cos(\frac{n_x\pi}{N_x+1}) + \cos(\frac{n_y\pi}{N_y+1}))$, where $n_x = 1, 2, \dots, N_x$ and $n_y = 1, 2, \dots, N_y$. Because the QD array is connected to the electrodes, these electronic states have inhomogeneous broadening. They are also restricted within the range between $-4t_c$ and $4t_c$. We can tune the distribution of electronic states by changing N , t_c and Γ_t .

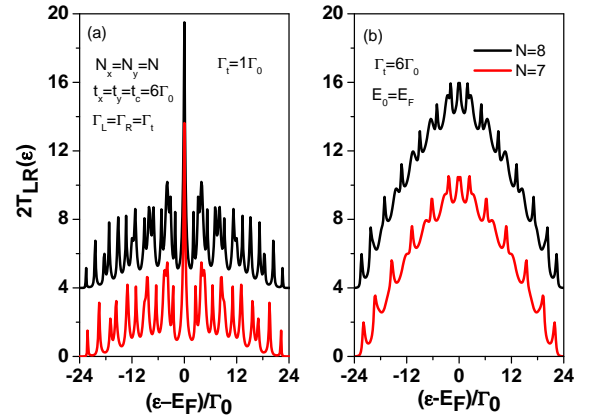


FIG. 2: Transmission coefficient $T_{LR}(\varepsilon)$ as a function of ε for different N values at $t_x = t_y = t_c = 6\Gamma_0$ and $E_0 = E_F$. Diagrams (a) and (b) consider tunneling rates $\Gamma_L = \Gamma_R = \Gamma_t = 1\Gamma_0$ and $\Gamma_t = 6\Gamma_0$, respectively. To prevent the curves from overlapping each other, we shifted the curve of $N = 8$.

From Eqs. (4) and (5), the maximum electron current and heat current occur at $T_{LR}(\varepsilon)$ with the maximum area. The authors of Ref. [24] proved two results: the maximum area of $T_{LR}(\varepsilon)$ can be reached at

the condition of $\Gamma_t = t_c$ and the maximum area increases with increasing N , as seen in Fig. 2(b). Note that the 2D tight-binding electronic states show the Van Hove singularity in the density of states (DOS) as $N \rightarrow \infty$ (DOS diverges at E_0). At zero temperature, the electrical conductance is given by the transmission coefficient $G_e = \frac{2e^2}{h} T_{LR}(E_F)$. We now clarify how the electronic states influence the thermoelectric coefficients of a finite 2D QD array.

Fig. 3 shows the calculated G_e , κ_e and Lorenz number ($L_0 = \kappa_e / (T G_e)$) at functions of the QD energy level for various values of Γ_t at $k_B T = 1\Gamma_0$, $t_c = 6\Gamma_0$ and $N = 8$. As a result of temperature effect ($\frac{\partial f(\varepsilon)}{\partial E_F}$), the electronic states shown in Fig. 2(a) can not be resolved in Fig. 3(a). It is not easy to justify a finite 2D QD array in the band-like or molecule-like situation from G_e at finite temperature, especially at high temperatures. The curves of κ_e in Fig. 3(b) are similar to those of G_e . According to the Wiedemann-Franz law, $L_0 / (k_B^2 / e^2) = \frac{\pi^2}{3}$ is a temperature-independent quantity. In Fig. 3(c), the L_0 curve corresponding to $\Gamma_t = 6\Gamma_0$ is approximately $\pi^2/3$. For comparison, we also add the calculated G_e , κ_e and L_0 for 1D QD array with $N_x = 100$ and $t_c = \Gamma_t = 12\Gamma_0$ (the band width of $48\Gamma_0$ in this 1D miniband). As seen in Fig. 3(c), 1D QD array yields a Lorenz number $L_0 = \frac{k_B^2}{e^2} \frac{\pi^2}{3}$ between $-10\Gamma_0 \leq \Delta \leq 10\Gamma_0$. This can be regarded as a manifested band-like transport.

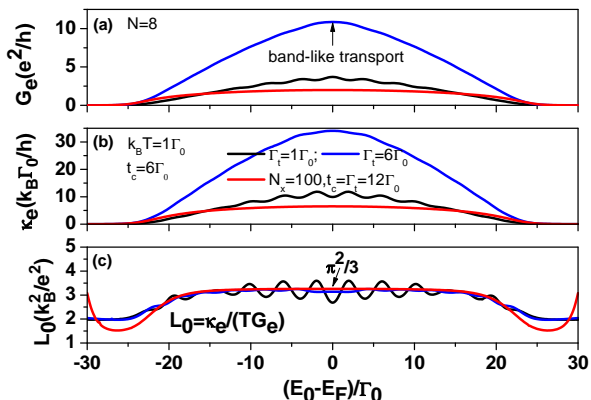


FIG. 3: (a) Electrical conductance G_e , (b) electron heat conductance κ_e and (c) Lorenz number ($L_0 = \kappa_e / (T G_e)$) as functions of $\Delta = E_0 - E_F$ for various Γ_t values at $k_B T = 1\Gamma_0$, $t_c = 6\Gamma_0$ and $N = 8$. The red curves correspond to a 1D QD array with $N_x = 100$, $t_c = \Gamma_t = 12\Gamma_0$ and $k_B T = 1\Gamma_0$.

Furthermore, we have calculated G_e , κ_e and L_0 for 2D QD array with $N = 8$ as functions of temperature for different Γ_t values at $E_0 = E_F$ and $t_c = 6\Gamma_0$ in Fig. 4. The red curves are the results of the 1D QD array corresponding to those of Fig. 3. One-dimensional QD arrays have a temperature-independent G_e and a linear temperature-dependent κ_e . As a consequence, $L_0 = \kappa_e / (T G_e)$ leads to a temperature-independent behavior. According to the

results of Figs. 3 and 4, the thermoelectric properties of 2D QD arrays with $t_c = 6\Gamma_0$, $\Gamma_t = 6\Gamma_0$ and $N = 8$ are very similar to those of 1D QD arrays with minibands. We deduce that finite 2D QD arrays have band-like characteristics when $t_c = \Gamma_t = 6\Gamma_0$ and $N = 8$.

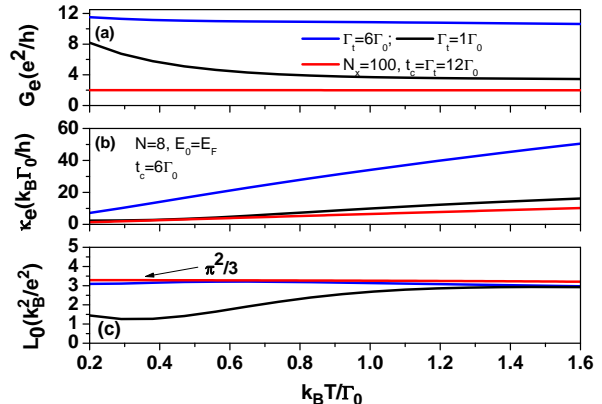


FIG. 4: (a) Electrical conductance, (b) electron heat conductance and (c) Lorenz number as functions of temperature for various Γ_t values at $E_0 = E_F$, $t_c = 6\Gamma_0$ and $N = 8$. The red curves correspond to those of Fig. 3 with $E_0 = E_F$.

Because many thermoelectric devices operate at high temperatures, it is important to examine the power factor of 2D QD arrays in this regime. In Figs. 2-4 we have focused on the electron transport in resonant tunneling procedure (RTP) in which the Seebeck coefficient is very small. To obtain a large PF value at high temperature, we considered the electron transport in the thermionic-assisted tunneling procedure (TATP) where the band center (E_0) is far away from the Fermi level E_F in the electrodes. In Fig. 5, we have calculated G_e , S , PF and L_0 as functions of temperature for various t_c values at $E_0 - E_F = 30\Gamma_0$. Because the maximum $T_{LR}(\varepsilon)$ area occurs at $\Gamma_t = t_c$, we adopted this condition for all the subsequent steps. As seen in Fig. 5(a), G_e is vanishingly small at low temperature due to the electronic states of 2D QD arrays being kept a certain distance from the E_F . The enhancement of G_e with increasing temperature is a typical characteristic arising from the TATP. To understand the temperature behavior of G_e at $\Gamma_t = t_c = 1\Gamma_0$, we have the expression of $G_{e,atom} = \frac{e^2}{h} \frac{\pi \Gamma_t}{2k_B T \cosh^2((E_0 - E_F)/(2k_B T))}$ when the transmission coefficient is approximated as $T_{LR}(\varepsilon) = 4\Gamma_t^2 / ((\varepsilon - E_0)^2 + (2\Gamma_t)^2)$ in Eq. (6). In addition, $S_{atom} = -\Delta/T = -(E_0 - E_F)/T$, which explains the behavior of S at $t_c = 1\Gamma_0$ and $k_B T \geq 2\Gamma_0$ in Fig. 5(b). Although G_e is highly enhanced with increasing t_c , S is not so sensitive to t_c for $k_B T \geq 10\Gamma_0$. This explains why the trend of maximum PF for t_c shown in Fig. 5(c) is determined by G_e . In Fig. 5(d), three L_0 curves violate the Wiedemann-Franz law. Note that $\Gamma_t = t_c = 6\Gamma_0$ provides the band-like characteristic (see Fig. 3(c)).

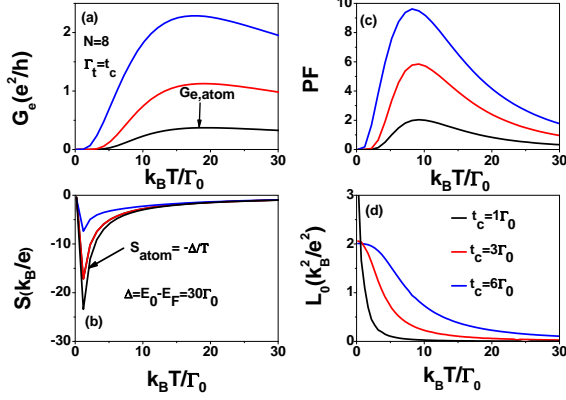


FIG. 5: (a) Electrical conductance, (b) Seebeck coefficient, (c) power factor ($PF = S^2 G_e$) and (d) Lorentz number as functions of T for various t_c values at $E_0 - E_F = 30\Gamma_0$ and $N = 8$. Meanwhile, we have adopted $\Gamma_t = t_c$.

Fig. 6 shows the calculated G_e , S and PF as functions of E_0 for various t_c values at $k_B T = 25\Gamma_0$ to reveal the effect of the band center. As seen in Fig. 6(a), G_e has a maximum value when the band center (E_0) is located at E_F . The Seebeck coefficients in Fig. 6(b) are zero at $E_0 = E_F$. It is attributed to the symmetrical distribution of the electrons and holes on the electronic states of the 2D QD array. Here, the holes are defined as the empty states below E_F . For $k_B T = 25\Gamma_0$, the Seebeck coefficients are well described by $S_{atom} = -\Delta/T$. We find that the maximum values of PF occur near $\Delta = 60\Gamma_0$, as indicated in Fig. 6(c). When approaching the atomic limit ($t_c \rightarrow 0$), one can prove that the optimization of PF is given by $\Delta/k_B T = 2.4$. The results of Fig. 6(c) imply that 2D QD arrays with minibands ($t_c = 6\Gamma_0$) preserve the atomic thermoelectric properties when the band center is far away from the E_F of the electrodes. In Fig. 2(b), $T_{LR}(\varepsilon)$ depends on N . Therefore, we add in Fig. 6 the curves with triangle marks for $N = 7$ and $t_c = 6\Gamma_0$. From the curves of $N = 7$ and $N = 8$, we see that the enhancement of G_e resulting from the increase of electronic states does not suppress S . It is worthy noting that a single 1D QD array does not exist such a behavior. We reinvestigate PF as functions of t_c for $N = 7, 8$ at $\Delta = 60\Gamma_0$ and $k_B T = 25\Gamma_0$ in Fig. 6(d). PF is a linear function of t_c as $t_c \leq 6\Gamma_0$. Meanwhile, the maximum PF is given by $t_c = \Delta/4$. The red curves represent the case where $t_y = 0$ to clarify the geometry effects. When $t_c \leq 6\Gamma_0$, the geometry effects can be ignored.

Because $T_{LR}(\varepsilon)$ lacks an analytical form, it is not easy to illustrate the complex behavior of PF shown in Fig. 6(d). If we make the assumption that minibands have homogenous electronic states and consider the square-form $T_{LR}(\varepsilon)$ given by

$$T_{LR}(\varepsilon) = \begin{cases} N_y & \text{if } -2t_c \leq \varepsilon - E_0 \leq 2t_c, \\ 0 & \text{otherwise} \end{cases} \quad (7)$$

the analytical forms of G_e and S can be derived as

$$G_e = \frac{2e^2 N_y}{h} (\tanh(y_1) - \tanh(y_2)) \quad (8)$$

and

$$S = \frac{2ek_B N_y}{h} \frac{(S_1(y_1) - S_2(y_2))}{G_e} \quad (9)$$

where $S_i(y_i) = y_i \tanh(y_i) - \log(\cosh(y_i))$, $y_1 = \frac{\Delta + 2t_c}{2k_B T}$ and $y_2 = \frac{\Delta - 2t_c}{2k_B T}$. In Fig 6(d), the blue curves are calculated by using Eqs. (8) and (9). Because Eq. (7) considers N_y 1D QD arrays with homogenous electric states, it is expected that the PF given by Eqs. (8) and (9) is overestimated. However, Eqs. (8) and (9) provide a clear picture that the enhancement of G_e . Meanwhile, $S \approx S_{atom}$ as long as $\frac{t_c}{k_B T} < 0.25$ and $\frac{\Delta}{k_B T} \geq 2.4$. We deduce that G_e in a band-like transport situation and S in an atomic-like situation can coexist for finite 2D QD arrays with $t_c = 6\Gamma_0$ and $\Delta = 60\Gamma_0$ at $k_B T = 25\Gamma_0$. If we set $\Gamma_0 = 1 \text{ meV}$, then our analysis in Fig. 6 becomes a very useful guideline for thermoelectric devices operated at room temperature.

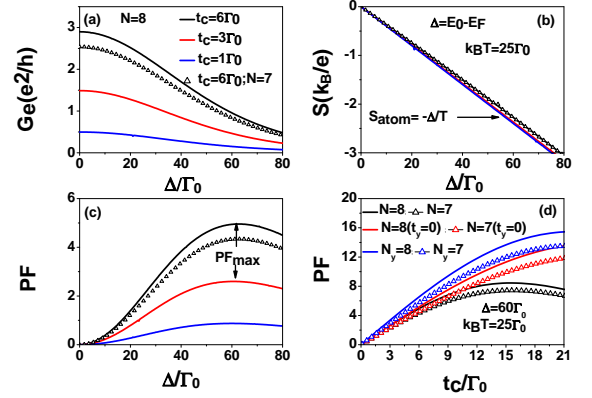


FIG. 6: (a) Electrical conductance, (b) Seebeck coefficient and (c) power factor as functions of E_0 for different t_c values at $N = 8$ and $k_B T = 25\Gamma_0$. The curves with black triangle marks correspond to the case of $N = 7$ and $t_c = 6\Gamma_0$. (d) PF as functions of t_c for $\Delta = 60\Gamma_0$ and $k_B T = 25\Gamma_0$. The red curves correspond to $t_y = 0$. The blue curves are calculated using Eq. (7).

IV. CONCLUSION

We have theoretically investigated the thermoelectric properties of 2D QD arrays. In RTP, the Lorenz number with a value near $\pi^2/3$ and a temperature-independent behavior demonstrates that 2D QD arrays with $t_c = \Gamma_t = 6\Gamma_0$ and $N = 8$ indeed form minibands. When this miniband center is far away from the Fermi level of the electrodes, TATP dominates the electron transport between

the electrodes and L_0 violates the Wiedemann-Franz law. In TATP, G_e is enhanced as the number of electronic states increases, whereas the S values remain in an atom-like situation. This is a remarkable property that would lead to a high-efficiency thermoelectric devices made of QDs with large electrical power output. This interesting phenomenon exists not only for 2D QD arrays with square-lattices but also triangular-lattices, which will be reported in elsewhere.

Acknowledgments

This work was supported under Contract No. MOST

107-2112-M-008 -023MY2

E-mail address: mtkuo@ee.ncu.edu.tw

Data Availability Statements

The data that supports the findings of this study are available within the article.

-
- ¹ L. J. Guo, E. Leobandung, and S. Y. Chou, *Science* **275**, 649 (1997).
- ² H. W. C Postma, T. Teepen, Z. Yao, M. Grifoni, and C. Dekker, *Science* **293**, 76 (2001).
- ³ S. Kubatkin, A. Danilov, M. Hjort, J. Cornil, J. L. Bredas, N. Stuhr-Hansen, P. Hedegard, and T. Bjornholm, *Nature* **425**, 698 (2003).
- ⁴ P. Michler, A. Imamoglu, M. D. Mason, P. J. Carson, G. F. Strouse, and S. K. Buratto, *Nature* **406**, 968 (2000).
- ⁵ C. Santori, D. Fattal, J. Vuckovic, G. S. Solomon, and Y. Yamamoto, *Nature* **419**, 549 (2002).
- ⁶ W. H. Chang, W. Y. Chen, H. S. Chang, T. P. Hsieh, J. I. Chyi, and T. M. Hsu, *Phys. Rev. Lett.* **96**, 117401 (2006).
- ⁷ S. Gustavsson, M. Studer, R. Leturcq, T. Ihn, K. Ensslin, D. C. Driscoll and A. C. Gossard, *Phys. Rev. Lett.* **99**, 206804 (2007).
- ⁸ M. Josefsson, A. Svilans, A. M. Burke, E. A. Hoffmann, S. Fahlvik, C. Thelander, M. Leijnse, H. Linke, *Nature Nanotechnology* **13**, 920 (2018).
- ⁹ C. R. Kagan and C. B. Murry, *Nature Nanotechnology* **10**, 1013 (2015).
- ¹⁰ T. C. Harman, P. J. Taylor, M. P. Walsh, and B. E. LaForge, *Science* **297**, 2229 (2002).
- ¹¹ E. Talgorn, Y. Gao, M. Aerts, L. T. Kunneman, J. M. Schins, T. J. Savenije, Marijn A. van Huis, Herre S. J. van der Zant, Arjan J. Houtepen and Laurens D. A. Siebbeles, *Nature Nanotechnology* **6**, 733 (2011).
- ¹² David. M.-T. Kuo and Y. C. Chang, *Phys. Rev. B* **81**, 205321 (2010).
- ¹³ R. S. Whitney, *Phys. Rev. Lett.* **112**, 130601 (2014).
- ¹⁴ David M. T. Kuo and Y. C. Chang, *Physica E* **115**, 113671 (2020).
- ¹⁵ G. Chen, *Phys. Rev. B* **57**, 14958 (1998).
- ¹⁶ G. Chen, M. S. Dresselhaus, G. Dresselhaus, J. P. Fleurial, and T. Caillat, *International Materials Reviews*, **48**, 45 (2003).
- ¹⁷ G. D. Mahan, L. M. Woods, *Phys. Rev. Lett.* **80**, 4016 (1998).
- ¹⁸ L. D. Lhao, S. H. Lo, Y. Zhang, H. Sun, G. Tan, C. Uher, C. Wolverton, V. P. Dravid and M. G. Kanatzidis, *Nature* **508**, 373 (2014).
- ¹⁹ C. Chang, M. Mu, D. He, Y. Pei, and C. F. Wu et al., *Science* **360**, 778 (2018).
- ²⁰ D. D. Fan, H. J. Liu, L. Cheng, P. H. Jiang, J. Shi and X. F. Tang, *Appl. Phys. Lett.* **105**, 133113 (2014).
- ²¹ H. Haug and A. P. Jauho, *Quantum Kinetics in Transport and Optics of Semiconductors* (Springer, Heidelberg, 1996).
- ²² D. M. T. Kuo, C. C. Chen and Y. C. Chang, *Phys. Rev. B* **95**, 075432 (2017).
- ²³ Y. Meir and N. S. Wingreen, *Phys. Rev. Lett.* **68**, 2512 (1992).
- ²⁴ D. M. T. Kuo, *AIP Advances* **10**, 045222 (2020).